Molecular Dynamics Simulations of Anharmonic Infrared Spectra of [SiPAH]+ π-Complexes

ARTICLE *in* THE JOURNAL OF PHYSICAL CHEMISTRY A · MAY 2010

Impact Factor: 2.69 · DOI: 10.1021/jp911526n · Source: PubMed

6 AUTHORS, INCLUDING:

Baptiste Joalland
Université de Rennes 1
24 PUBLICATIONS **80** CITATIONS

SEE PROFILE

Molecular Dynamics Simulations of Anharmonic Infrared Spectra of $[SiPAH]^+$ π-Complexes

B. Joalland,*,†,‡,§,∥ M. Rapacioli,§,∥ A. Simon,§,∥ C. Joblin,†,‡ C. J. Marsden,§,∥ and F. Spiegelman§,∥

Université de Toulouse, UPS, Centre d'Etude Spatiale des Rayonnements, Observatoire Midi-Pyrénées, 9 Av. du Colonel Roche, F-31028 Toulouse cedex 04, France, CNRS, CESR, F-31028 Toulouse cedex 04, France, Université de Toulouse, UPS, Laboratoire de Chimie et Physique Quantiques, IRSAMC, 118 Route de Narbonne, F-31062 Toulouse, France, and CNRS, LCPQ, IRSAMC, F-31062 Toulouse, France

Received: December 4, 2009; Revised Manuscript Received: March 3, 2010

This paper presents an investigation of anharmonic effects in the IR spectra of $[SiPAH]^+$ complexes by using Born−Oppenheimer molecular dynamics for a variety of PAHs ranging from naphthalene ($C_{10}H_8$) to ovalene ($C_{32}H_{14}$). The potential energy surfaces are calculated with the self-consistent charge density functional-based tight binding approach (DFTB). The DFTB parameters are modified to reproduce potential energy surfaces and the harmonic infrared spectra of the studied complexes with respect to DFT calculations. For bare PAHs, we find that the evolution of the vibrational frequencies of the C−H out-of-plane bending and C−C stretching modes as a function of temperature follows a linear law in quantitative agreement with experimental data. For cationic PAHs, the anharmonicity of the bands in terms of position shifts is found to be enhanced with respect to that of neutrals. As compared with bare cationic PAHs, the coordination of Si induces (i) larger broadenings, (ii) a slightly larger shift of the C−C stretching mode, and (iii) a smaller shift of the C−H out-of-plane bending modes. We discuss the implications of the work and the spectroscopic constraints for the detection of $[SiPAH]^+$ in the interstellar medium.

Introduction

Polycyclic aromatic hydrocarbons (PAHs) and PAH-related molecules are today largely admitted as an important component of the interstellar matter, as containing more than 15% of the cosmic carbon.[1] They have been proposed as the carriers of the aromatic infrared bands (AIBs) that illuminate the general interstellar medium (ISM) of galaxies[2,3] and are located at 3.3, 6.2, 7.7, 8.6, 11.2, and 12.7 μm (3030, 1610, 1300, 1160, 890, and 790 cm^{-1}). Interstellar PAHs offer a large surface for atomic and molecular adsorptions. Elemental silicon being strongly depleted from the gas-phase in the ISM,[4] a significant fraction of this element is likely to be involved in the formation of complexes with PAHs.[5] Gas-phase experimental studies have shown that (i) the capture of the ground state atomic silicon ions Si^+ (^2P) by small aromatic molecules to form complexes is an efficient process[6−10] and (ii) the large PAH molecular surface could play a catalytic role in the formation of small Si-bearing molecules of astrophysical interest.[11]

In previous work,[5] we studied a variety of model $[SiPAH]^+$ complexes at the density functional theory (DFT) level. We characterized their structures and showed that $[SiPAH]^+$ complexes are thermodynamically stable. Computation of harmonic IR spectra revealed that Si coordination could account for some AIB features (blueshift of the 6.2 μm band and presence of two satellite bands of the 6.2 and 11.2 μm AIBs). However, the calculated spectra correspond to IR emission at 0 K, whereas astronomical spectra result from the emission of hot species. The population of these hot vibrational levels results from sequential processes involving initial electronic excitation via UV photons followed by a relaxation to the ground state with a large energy excess. Relaxation then proceeds through the emission of IR photons.[12]

In the hot emitting PAHs, anharmonic effects entail band shifts and broadenings.[13−21] Similar effects are expected for $[SiPAH]^+$ complexes that present additional soft and anharmonic modes corresponding to Si motions over the PAH surface. The present study aims at investigating the variations of $[SiPAH]^+$ IR spectra as a function of temperature.

For small systems, almost exact quantum dynamical calculation of vibrational states can be achieved either with wavepacket techniques, vibrational complete active space SCF,[22] multiconfiguration time-dependent hartree[23−25] approaches, and sometimes quantum path integral methods. Other recent approaches use anharmonic high-order force field constants obtained by DFT calculations,[26] coupled with descriptions of energy and thermal populations in the vibrational levels.[13,14] For larger systems, the frequencies of the fundamental vibrations in IR spectra are often estimated by scaling the harmonic frequencies.[27] However, anharmonic effects in the classical approximation can be obtained by Born−Oppenheimer[28] or Car−Parrinello[29,30] molecular dynamics (MD). This is what is used in the present study, where we perform Born−Oppenheimer MD simulations and calculate the spectra through a dipole autocorrelation function. To run long MD simulations on $[SiPAH]^+$ complexes containing up to 47 atoms, one needs a computer-efficient calculation of the potential energy function. We use here a self-consistent charge density functional based tight binding (SCC-DFTB) approach.[31−34] This method is an approximate DFT scheme with a low computa-

* To whom correspondence should be addressed E-mail: baptiste.joalland@cesr.fr.
† Université de Toulouse, UPS, Centre d'Etude Spatiale des Rayonnements.
‡ CNRS, CESR.
§ Université de Toulouse, UPS, Laboratoire de Chimie et Physique Quantiques.
∥ CNRS, LCPQ, IRSAMC.

10.1021/jp911526n
Published on Web 04/15/2010

tional time that has been widely used to describe a variety of large molecular systems.[34]

In the next section, after a brief introduction to SCC-DFTB and its specific parametrization for the present work, we describe the IR spectra calculation procedure. In Section 3, we present and discuss the computed spectra for cationic complexes of silicon with naphthalene ($C_{10}H_8$), pyrene ($C_{16}H_{10}$), coronene ($C_{24}H_{12}$), and ovalene ($C_{32}H_{14}$).

Method and Parameters

Potential Energy Surface Description. ***DFTB Potential.*** An exhaustive description of the SCC-DFTB method can be found in refs 31−34. Briefly, this method is based on the three following approximations:

(i) The Kohn−Sham energy is developed up to the second order around a reference density leading to:

$$E^{\mathrm{SCC-DFTB}} = \sum_{i}^{\mathrm{occ}} n_i \langle \varphi_i | \hat{h}_0 | \varphi_i \rangle + \sum_{\alpha,\beta \neq \alpha}^{\mathrm{atoms}} E^{\mathrm{rep}}(R_{\alpha\beta}) + \frac{1}{2} \sum_{\alpha\beta}^{\mathrm{atoms}} \gamma_{\alpha\beta}(R_{\alpha\beta}) \delta q_\alpha^{\mathrm{Mull}} \delta q_\beta^{\mathrm{Mull}} \quad (1)$$

In the first term, φ_i are the Kohn−Sham molecular orbitals, $\hat{h}_0$ is the monoelectronic Hamiltonian at the reference density, and n_i is the occupation number. The second term E_{rep} is a repulsive contribution expressed as a sum of atomic-pair terms. The third term is the second-order term expressed as a function of Mulliken atomic charges fluctuation $\delta q_\alpha^{\mathrm{Mull}}$ and $\gamma_{\alpha\beta}$ atomic pair fitted functions.

(ii) The molecular orbitals are expressed as linear combinations of atomic orbitals with a minimal atomic basis set of ϕ_μ functions:

$$\varphi_i = \sum_\mu c_{i\mu} \phi_\mu$$

(iii) All the three-center contributions are neglected in the Kohn−Sham matrix.

As a consequence, this approximate DFT method allows a significant gain in terms of computational time as compared to DFT, since no integral is explicitly calculated and the diagonalizations performed in the self-consistent process involve a reduced basis set. As mentionned in the introduction, this reduced computational time is essential if molecular dynamics calculations on PAH complexes are to be achieved.

Parametrization. DFTB parameters are usually developed with the focus of reproducing a large variety of systems from crystals to molecules rather than giving a precise description of some specific systems as required in the present study. We have thus modified the default atomic DFTB parameters that involve silicon[35,36] to reproduce the optimized geometries, binding energies and charge distribution of DFT calculations obtained with the B3LYP functional and the D95++** basis set.[5] At this level, the dissociation energies of [Si-PAH]$^+$ complexes into Si + PAH$^+$ lie in the [1.6−2.7] eV range depending on the PAH size. The global minima correspond to structures where the Si atom is either located above a C−C bond ([$SiC_{10}H_8$] $^+$), adsorbed on a perihedral carbon atom ([$SiC_{16}H_{10}$]$^+$ and [$SiC_{24}H_{12}$]$^+$) or coordinated with an external C atom and two H atoms in ([$SiC_{32}H_{14}$]$^+$), as can be seen in Figure 1.

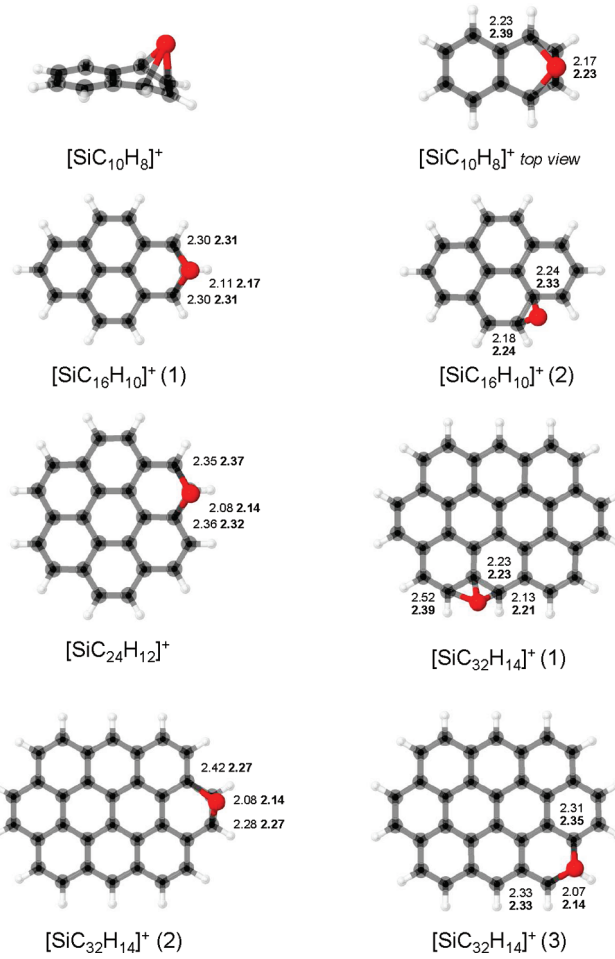

Figure 1. Lower-energy isomers for the [SiPAH]$^+$ complexes including naphthalene ($C_{10}H_8$), pyrene ($C_{16}H_{10}$), coronene ($C_{24}H_{12}$), and ovalene ($C_{32}H_{12}$). Geometries are optimized at the B3LYP/D95++** level of theory. The values (in Å) correspond to the Si−C bond lengths with B3LYP/D95++** (normal font) and SCC-DFTB† respectively (bold font).

The lowest energy structures at the SCC-DFTB level using the default parameters are slightly distorted with respect to the DFT ones and have higher binding energies (2.9 eV instead of 2.1 eV at the DFT level for pyrene). In the case of [$SiC_{16}H_{10}$]$^+$, a DFT Mulliken population analysis indicates that 87% of the charge is carried by the PAH but only 72% with SCC-DFTB. One may relate this discrepancy to a general deviation of the SCC-DFTB differences between the ionization potentials (IP), namely Δ(IP) = IP(PAH) − IP(Si). Indeed, the latter values lie more than 1 eV higher than both the experimental and DFT ones (see Figure 2).

In the context of ab initio density functional framework, such problem may be solved by complementing the basic Kohn−Sham equations with a Hubbard-inspired term, as in the LDA+U method,[37,38] which brings on-site correlation corrections to the mean field Kohn−Sham equation and modified one-electron energies (for a review see for instance Kotliar et al.[39]). This provides a better determination of the HOMO−LUMO gap, conditioning the charge balance and the conduction properties that are especially important in iono-covalent materials. The method proves quite efficient for some classes of materials, although it is dependent on the various schemes used to avoid double counting. In the present parametrized approach, we have chosen a more phenomenological correction consisting in altering the unperturbed atomic orbital energies. This was also

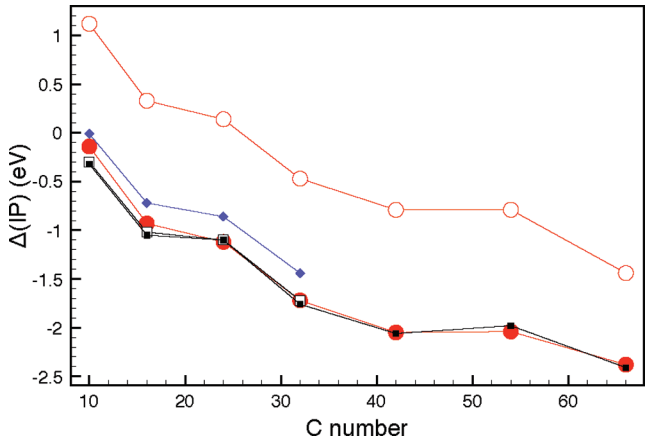

Figure 2. Experimental and calculated values of the ionization potential differences Δ(IP) (eV) = IP(PAH) − IP(Si). Circles: SCC-DFTB calculations with (filled) and without (open) AOE correction. Squares: DFT calculations at the B3LYP/D95++** (small) and B3LYP/6-31+G* (large) levels of theory. Diamonds: experimental values.

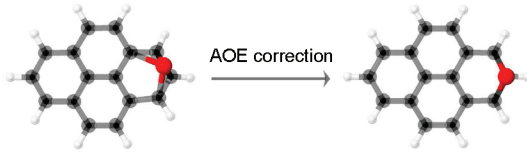

Figure 3. $[SiC_{16}H_{10}]^+$ lowest energy isomers with the SCC-DFTB approach with (right) and without (left) AOE correction.

TABLE 1: Binding Energies (E_b) of the Lowest Energy $[SiPAH]^+$ Isomers with Respect to the Most Stable Dissociation Products ($Si(^3P) + PAH^+$)

			E_b (eV)		
			SCC-DFTB AOE correction	SCC-DFTB†	B3LYP[a]
$[SiC_{10}H_8]^+$		$^2A'$	3.58	2.50	2.67
$[SiC_{16}H_{10}]^+$	(1)	^2A	2.94	2.08	2.08
	(2)	^2A	2.73	1.90	1.86
$[SiC_{24}H_{12}]^+$		^2A	2.88	1.97	1.95
$[SiC_{32}H_{14}]^+$	(1)	^2A	2.60	1.71	1.69
	(2)	^2A	2.53	1.62	1.58
	(3)	^2A	2.51	1.58	1.57

[a] Joalland et al.[5]

easier since we use here charges condensed to atoms and not charges condensed to atomic orbitals as in the LDA+U expressions. The application of a common shift of 1.26 eV to the SCC-DFTB Si atomic orbitals energies (AOE correction) enables the DFT Δ(IP) for a large sample of PAHs to be reproduced. Actually, this corrects the Si-PAH charge transfer and appears to better reproduce the DFT optimized structures (Figure 3 illustrates the $[SiC_{16}H_{10}]^+$ case where 88% of the charge is now carried by the PAH). It should be noticed that the IPs of isolated PAHs already have an evolution similar the DFT ones and those obtained from experiment. Although this modification allows to correct the geometries, the Si-PAH binding energies E_b remain about 1 eV above the DFT values (cf. Table 1) and the Si−C binding distances still have to be improved in particular for the second Si−C neighbors. To overcome these discrepancies, we modified the Hamiltonian off-diagonal matrix elements involving Si and C orbitals. Applying a constant scaling factor (0.9) allows for the reproduction of the DFT E_b value in the $[SiC_{16}H_{10}]^+$ complex, but the distances between Si and its C second neighbors remain too small. The application of a scaling factor evolving with the R_{SiC} distance from 0.9 for the nearest neighbors to 0.85 for the second neighbors is described by the formula $0.9 - 0.05/(1 + \exp(-20((R_{SiC}(Å))/(2.6) - 1)))$ and allow ther reproduction of the DFT optimized geometry. As a result, the empirically scaled parameter SCC-DFTB, hereafter labeled SCC-DFTB†, leads to binding energies and geometries very close to those obtained at the DFT level for a variety of $[SiPAH]^+$ complexes (see Table 1 and Figure 1).

Figure 4 shows the energetic profile of a characteristic Si diffusion above $C_{24}H_{12}^+$ calculated with DFT and SCC-DFTB† levels of theory, respectively. The Si atom is kept at 2 Å above the PAH plane, a typical distance in these complexes. The DFT and SCC-DFTB† profiles have similar behaviors when the Si atom is on the edge of the PAH (points 0−15). As compared with DFT, the SCC-DFTB† approximation underestimates the energies corresponding to the diffusion on the inner C-skeleton (points 15−30) or above the aromatic ring center (points 30−50). However, for the range of energies investigated in the MD simulations presented in Section 3, the Si motion is mainly localized at the edge of the PAH (for instance, the Si atom remains on the PAH edge more than 95% of the time during a simulation of 1 ns at ∼800 K). The PES is correctly reproduced on the PAH edge, a very flat region of primary interest in term of Si occupation.

Spectroscopy. The harmonic modes are obtained by diagonalizing the Hessian matrix at the optimized geometries. The

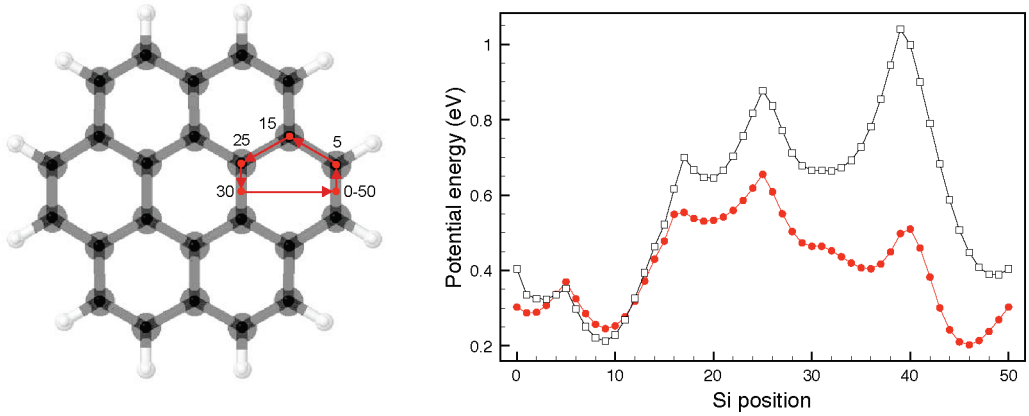

Figure 4. Potential energy profiles for diffusion of Si on PAH surface along characteristic paths at the SCC-DFTB† (filled circles) and B3LYP/D95++** (open squares) levels of theory. The Si atom lies 2 Å above the PAH plane. DFT and SCC-DFTB† optimized structure energies are taken as the zero-energy reference. Labels 0 and 50 correspond to the same Si position.

intensities are proportional to the squared module of the dipole moment derivative with respect to the normal modes coordinates.

Dynamical spectra are calculated by Fourier transform of the dipole−dipole time autocorrelation function.[40] The infrared absorption coefficient, $\alpha(\omega)$ is:

$$\alpha(\omega) = \frac{2\pi\omega(1 - e^{-\beta\hbar\omega})D(\omega)}{3\hbar c}\int_{-\infty}^{+\infty} dt\langle\mu(0)\mu(t)\rangle e^{i\omega t} \quad (2)$$

where $\beta = 1/(kT)$, with k being the Boltzmann constant, T being the temperature, c is the speed of light, and $\mu(t)$ is the molecular dipole moment at time t. $\langle\mu(0)\mu(t)\rangle$ indicates a statistical average over the simulations to avoid dependencies on the initial conditions. $D(\omega)$ corrects for the violation of the detailed balance conditions in classical MD and for hydrogen atom zero-point motion effects. Among common choices for this quantum correction factor, the $\beta\hbar\omega/(1 - e^{\beta\hbar\omega})$ expression, which corresponds to the combination of the desymetrization detailed balance factor $2/(1 + e^{-\beta\hbar\omega})$ with the hydrogen zero-point motion correction $\beta\hbar\omega/(2\tanh(\beta\hbar\omega/2))$, gives reasonable results for dynamical spectra at low temperatures as compared with harmonic spectra derived from the Hessian matrix (for further details see appendix of Gaigeot and Sprik[30]). Finally, the absorption coefficient is given by:

$$\alpha(\omega) \propto \omega^2\int_{-\infty}^{+\infty} dt\langle\mu(0)\mu(t)\rangle e^{i\omega t} \quad (3)$$

The SCC-DFTB† MD simulations were performed in the microcanonical ensemble using a time step of 1 fs. For each total energy, the molecular dynamics started from one initial configuration corresponding to the lowest isomer, the energy excess being given under kinetic energy form. Although we achieved here microcanonical simulations, we discussed our results in terms of temperatures estimated from the mean kinetic energy $\langle E_k\rangle$ during the dynamics

$$T = 2\frac{\langle E_k\rangle}{(3n - 6)k}$$

n being the total number of atoms. As the Si atom tends to detach from the PAH at high temperatures, the simulation temperature range was limited to [10−900] K for all complexes except $[SiC_{32}H_{14}]^+$, for which detachment was found to occur at rather low energy ($T = 600$ K). For each energy, the spectra result from five molecular dynamic runs of 100 ps each. These spectra will be discussed in the following as a function of the kinetic temperature.

At the higher temperatures explored here and even with the sampling used in the work, the simulated spectra turned out to be somewhat noisy. To smooth the signal, all dynamical spectra were convoluted by a Lorentzian profile of full width at half-maximum (fwhm) depending on the temperature using a linear expression. This expression is analogous to that of ref 41 describing the full width as derived from experiments on gas-phase neutral PAHs ($\Delta\nu(T) = \Delta\nu^{0K} + \chi' T$), but with different χ' constants, since its purpose here is to smooth the noise, the physical width being actually obtained via molecular dynamics. Bandwidths in the convoluted spectra have been checked to be representative of the dynamics at finite temperature and not of the convolution function.

TABLE 2: Total Dipole Moments in Debye of Benchmark Planar [SiPAH]$^+$ Complexes[a]

		B3LYP D95++**	SCC-DFTB† CM3 D_{CH}	SCC-DFTB† CM3 $D_{CH}D_{SiC}$
$[SiC_{10}H_8]^+$		4.31	4.07	5.67
$[SiC_{16}H_{10}]^+$	(1)	4.17	3.63	5.54
	(2)	4.51	3.94	5.52
$[SiC_{24}H_{12}]^+$		7.93	7.39	8.24
$[SiC_{32}H_{14}]^+$	(1)	3.47	2.71	4.32
	(2)	6.25	4.30	6.34
	(3)	6.57	4.24	6.32

[a] The origin is the mass center of each complex.

In a DFT calculation, the dipole moment of a system is derived from the electronic density calculated on a grid or on an explicit basis. In standard DFTB, two approximations are used (i) the dipole moment is calculated from atomic point charges and (ii) these charges are derived from the density matrix with the Mulliken definition. Kalinowski et al.[42] have shown that the calculation of molecular dipole moments with SCC-DFTB can be improved by using atomic charges obtained from the CM3 charge model approach,[43−45] instead of using Mulliken's.

The CM3 charges are defined by

$$q_k^{CM3} = q_k^{Mull} + \sum_{k\neq k'}^{atoms}[D_{ZkZk'}B_{kk'} + C_{ZkZk'}B_{kk'}^2] \quad (4)$$

where $B_{kk'}$ is Mayer's bond order defined by

$$B_{kk'} = \sum_{\lambda\in k}^{atoms}\sum_{\omega\in k'}^{atoms}(\mathbf{PS})_{\omega\lambda}(\mathbf{PS})_{\lambda\omega} \quad (5)$$

P and **S** are density and atomic basis overlap matrices. $C_{ZkZk'}$ and $D_{ZkZk'}$ are empirical parameters determined for each atomic pair of non-identical atoms. To some extend, this formula can be understood as a modification the Mulliken point charges, introducing an extra bond dipole with charge separation equal to the bond distance.

For the C−H bond, we use the parametrization of Rapacioli et al.[46] For the Si−C bonds, DFT dipoles were calculated for a set of [SiPAH]$^+$ complexes. To circumvent the differences resulting from different PAH deformations (in SCC-DFTB† vs DFT), the benchmark complexes are composed of a planar PAH with a Si atom 2 Å above the plan, located above same carbon atom as in the true optimized geometry. The D_{SiC} parameter is derived to minimize the root-mean-square deviation between DFT total dipoles and those calculated with SCC-DFTB† and the CM3 D_{CH} parameter (see Table 2). We use the linear expression for the CM3 charges: $C_{SiC} = 0$ and $D_{SiC} = 0.14$. Despite the least-squares fitting process, this D_{SiC} parameter induces an overestimation of the total dipole moments of the smallest complexes with naphthalene and pyrene, whereas the agreement is significantly improved for the largest ones. This feature might be connected with the Δ(IP) difference between Si and PAH values that better match the DFT ones for complexes formed with larger PAHs than for naphthalene and pyrene (see Figure 2). The general trend with size is, however, satisfactory. Finally, the CM3 charges are only used to determine the mode intensities and take no part in the determination of the potential energy surface.

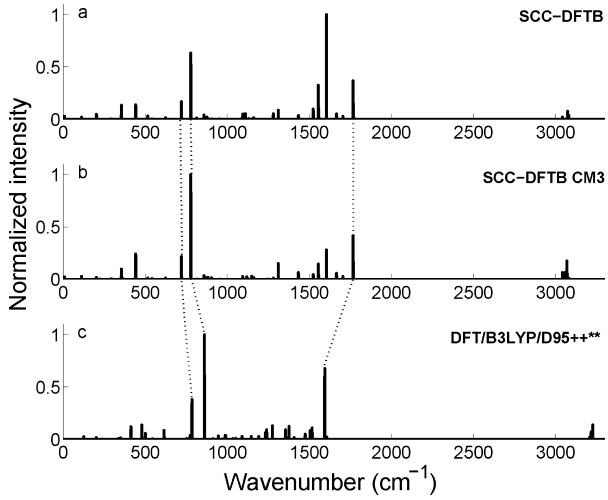

Figure 5. Harmonic spectra of $[SiC_{10}H_8]^+$. (a) SCC-DFTB† with Mulliken charges; (b) SCC-DFTB† with CM3 charges; and (c) B3LYP/D95++**. Dashed lines link the two γ_{CH} and the ν_{CC} modes.

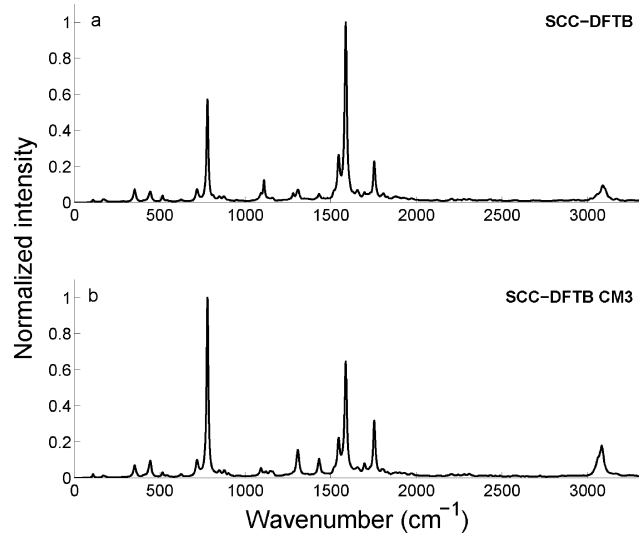

Figure 6. Anharmonic spectra of $[SiC_{10}H_8]^+$ at 300 K. (a) SCC-DFTB† with Mulliken charges; and (b) SCC-DFTB† with CM3 charges.

Note that the use of point charge may also be a limitation for the accuracy of electrostatic forces. More sophisticated force fields can be used including multipole distributions on atoms and bonds. Such multipole distributions certainly improve the description of intermolecular electrostatic interactions.[47−53] They are often used in the context of interactions between rigid molecules and are not straightforward to include in a self-consistent charge-based DFTB scheme.

Results

Harmonic SCC-DFTB† Spectra: Description of Normal Modes. The harmonic spectra of $[SiPAH]^+$ complexes obtained at the B3LYP/D95++** level have been extensively described elsewhere.[5] In the following section, only the $[SiC_{10}H_8]^+$ spectrum is discussed. The soft modes due to the Si motion are found at 202, 240, and 413 cm^{-1}. The first two correspond to Si motion essentially parallel to the PAH plane and have very low intensities, less than 2% of the maximum intensity (C−H mode at 862 cm^{-1}). The 413 cm^{-1} mode corresponds to a Si motion in a direction perpendicular to the PAH plane with an intensity of ∼12% of the maximum intensity.

In the mid-IR region, the neutral $C_{10}H_8$ spectrum is dominated by an out-of-plane C−H bending mode (γ_{CH}) and an in-plane C−H stretching mode (ν_{CH}), whereas the cationic $C_{10}H_8^+$ spectrum is dominated by the γ_{CH} mode and strong features in the 1200−1600 cm^{-1} range, corresponding to in-plane C−H bending modes (δ_{CH}) and in-plane C−C stretch modes (ν_{CC}). This is also the case for $[SiC_{10}H_8]^+$, with the charge being mainly localized on the PAH (cf. Figure 5). In the complex, however, a significant difference stems from the fact that the symmetry is reduced, due to the presence of the Si atom. The γ_{CH} band (located at 780 cm^{-1} in $C_{10}H_8^+$) is thus split into two subbands at 862 and 786 cm^{-1}. The first one, labeled $(CH)_{Si}$, involves mainly the bending of C−H bonds on the ring neighboring the Si atom, and the second one results from the other ring and is therefore less perturbed. The 1594 cm^{-1} band is assigned to a ν_{CC} mode that involves the whole PAH skeleton. It is blueshifted by 29 cm^{-1} with respect to that in $C_{10}H_8^+$. As discussed in our previous paper,[5] the splitting of the γ_{CH} band into two bands, as well as the blueshift of the ν_{CC} band, is a signature for the presence of $[SiPAH]^+$ complexes in the interstellar space.

The harmonic spectrum obtained at the SCC-DFTB† level using Mulliken and CM3 charges (cf. Figure 5, panels a and b, respectively) exhibits (i) soft Si-PAH modes at 203, 226, and 365 cm^{-1}, (ii) two γ_{CH} bands at 721 and 778 cm^{-1}, and (iii) a ν_{CC} band at 1767 cm^{-1}. Overall, the γ_{CH} modes are displayed at lower wavenumbers (∼75 cm^{-1}) and the ν_{CC} modes at higher wavenumbers (∼ 170 cm^{-1}) than at the DFT level. We point out that these discrepancies between SCC-DFTB† and DFT band positions are already observed on bare PAHs. For instance, in the B3LYP/D95++** harmonic spectrum of bare $C_{10}H_8$, the main γ_{CH} and ν_{CC} bands are located at 805 and 1639 cm^{-1} respectively. At the SCC-DFTB level, these positions are shifted to 763 and 1815 cm^{-1}. For comparison, the main γ_{CH} and ν_{CC} vibrations of $C_{10}H_8$ were recorded in a cold Ar matrix at 783−788 and 1604 cm^{-1}.[54] To reach the experimental frequencies, one must multiply the DFT values by a unique scaling factor of 0.98. Alternatively, in the SCC-DFTB scheme, the γ_{CH} and ν_{CC} have to be multiplied by different scaling factors of 1.03 and 0.88 respectively.

In the harmonic spectrum calculated with Mulliken charges (cf. Figure 5a), the most intense band lies at 1604 cm^{-1} and corresponds to an in-plane C−C vibrational mode. Its intensity is overestimated with respect to the DFT results. This affects the relative intensities of the whole spectrum. Along the normal coordinate associated with this vibrational mode, the charge variations are on average reduced with the CM3 approach (versus Mulliken), whereas the contrary is observed for the most intense γ_{CH} band at 778 cm^{-1} and the ν_{CC} band at 1767 cm^{-1}. Thus, calculating the harmonic intensities with a molecular dipole derived from CM3 charges (instead of Mulliken charges) improves the relative intensities of the spectrum as compared with DFT results (cf. Figure 5).

The $[SiC_{10}H_8]^+$ anharmonic spectra computed with Mulliken or CM3 point charges at 300 K are reported in Figure 6, panels a and b, respectively. In the simulation, the CM3 charge definition enhances the charge fluctuations between the Si atom and the PAH by ∼18%, as compared to Mulliken charge fluctuations. The resulting spectrum exhibits relative band intensities close to those calculated in the harmonic approximation (cf. Figure 5). In particular, the $(C-H)_{Si}$ out of plane bending band, characteristic feature of the Si coordination, is the most prominent one. In the following, all molecular dipoles are computed with CM3 charges.

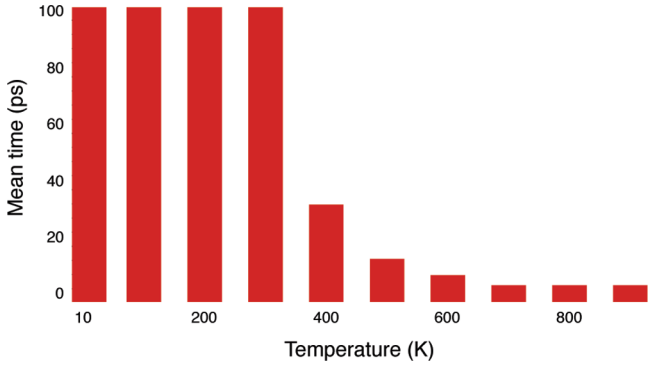

Figure 7. Mean time of continuous residence on a ring extracted from five simulations of 100 ps at each temperature.

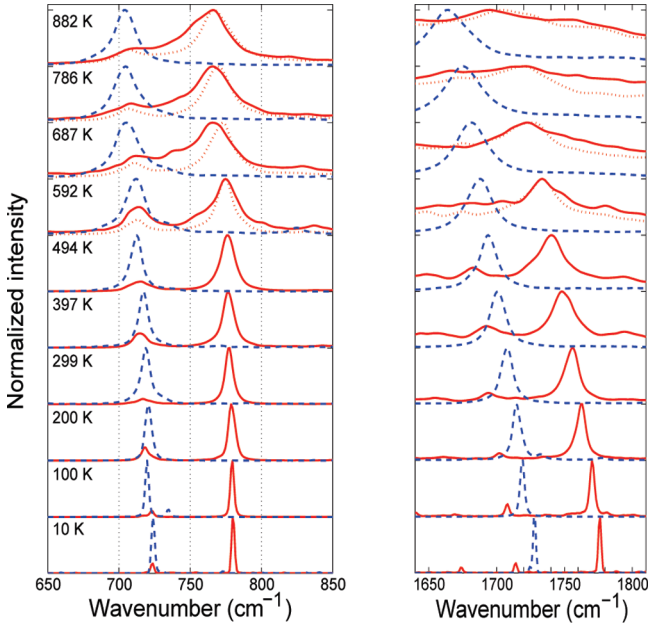

Figure 8. γ_{CH} (left) and ν_{CC} (right) band as a function of the temperature for $C_{10}H_8^+$ (dashed lines) and $[SiC_{10}H_8]^+$ (continuous line). For $T = 600-900$ K, the spectra of the Si-trapped complex (dotted line) is added (see text).

Influence of Temperature on the $[SiC_{10}H_8]^+$ Spectrum. ***Analysis of the Dynamics.*** The PES of $[SiC_{10}H_8]^+$ has two degenerate minima, corresponding to the coordination of the Si atom on top of each ring (Figure 1). For dynamical runs with sufficient kinetic energy, the Si atom oscillates between these two minima. Figure 6 represents the time of continuous residence on a given ring. Three different regimes can be observed. For temperatures below 400 K, the Si atom remains on top of the same ring for all the trajectories. Between 400 and 600 K, there is sufficient energy for the Si atom to overcome the barrier separating the two PES minima and the average time spent on a given ring decreases as the temperature increases. This is the "transient regime". For temperatures above 600 K, the complex reaches a "high temperature mobility" regime where the Si atom remains 2 ps on average on one ring.

Evolution of the C−H Out-of-Plane Bending Motion. As can be seen in Figure 8 for the naphthalene cation $C_{10}H_8^+$, the γ_{CH} band exhibits a broadening and a redshift when the temperature increases. The same behavior is observed in the $[SiC_{10}H_8]^+$ complex for the two γ_{CH} bands that result from the splitting due to the Si coordination. However, the broadening is much more significant for temperatures larger than 600 K (cf. Figure 8), which is when the system reaches the high temperature mobility regime.

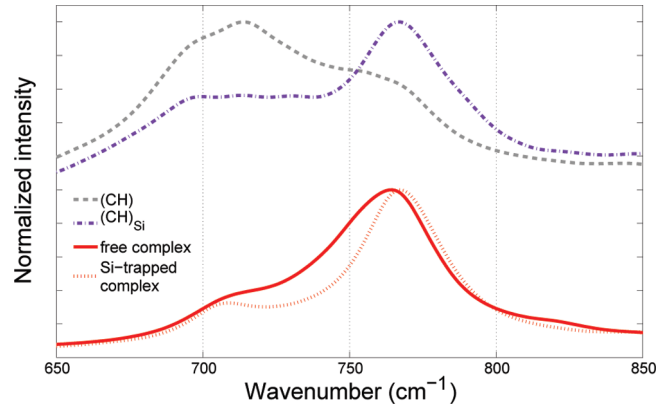

Figure 9. $[SiC_{10}H_8]^+$ γ_{CH} bending modes at 900 K. (i) bottom: free complex and Si-trapped complex; and (ii) top: contributions of the perturbed $(C-H)_{Si}$ and nonperturbed (C−H) out-of-plane bending motions.

To test the assumption that the Si atom transfers from ring to ring is at the origin of the γ_{CH} band broadening and eventually merging, we performed artificial simulation on a modified PES in order to inhibit such transfers. We added a nonphysical contribution to the potential of the form $\sum_j (2\text{ eV})/(|\mathbf{R}_{Si} - \mathbf{R}_{C_j}|^2)$ where the sum runs over the central carbon atoms of the naphtalene. This potential acts as a trap and prevents the Si atom from moving from one ring to the other, even at high temperature. The spectra obtained for dynamics ranging from 600 to 900 K with this modified potential are shown in Figure 8. The γ_{CH} band is now as broad as in the isolated PAH, which confirms that the more extensive broadening of this band in the complex is due to the Si motion between the two rings. Such IR band broadening due to conformational dynamics has already been described for other systems, as for instance compounds of biological interest.[55−57]

To investigate further the origin of the different contributions to this feature, we simulated two IR spectra using in eq 3 the autocorrelation of the dipole moment reduced to either its contribution on the C−H dipoles of the ring neighboring the Si atom, or to its contribution on the other cycle C−H dipoles. The two spectra resulting from dynamics at 900 K are presented in Figure 9. The bands are closer to each other compared to those obtained with a dynamics where the Si atom is trapped on one ring. In fact, at this temperature, the Si oscillation between the two rings is too fast (~2 ps, see Figure 7) to let the C−H modes reach the regime they have in the Si-trapped simulation. The two bands are thus shifted toward each other, each one displaying a broad wing in the interband region.

Evolution of the C−C Stretching Motion. For the $C_{10}H_8^+$ cation, the ν_{CC} band is also red-shifted and broadened when the temperature increases (see Figure 8). In the complex, this band roughly follows the same trend in terms of position and presents a wider broadening than in the bare PAH cation for temperatures larger than 400 K.

Trapping the Si atom on top of one ring using the artificial potential described previously scarcely affects the spectrum (cf. Figure 8, right), which means that the C−C in-plane stretch is barely sensitive to the motion of the Si atom above the PAH surface. This can be rationalized as the C−C stretching vibration is an in-plane delocalized mode sensitive to the global perturbation of the aromatic electronic system whatever the position of the Si atom. In contrast, the C−H mode is an out-of-plane motion, mechanically hindered by the presence of an Si atom.

TABLE 3: Anharmonicity Factors (χ) of the γ_{CH} and ν_{CC} Modes Derived from Molecular Dynamics Simulations ($\chi_{SCC-DFTB}$) for a Series of $PAH^{0/+}$ and $[SiPAH]^+$ Complexes, Performed between 10 and 900 K[a]

		γ_{CH}		ν_{CC}	
		$\chi_{SCC-DFTB}$ (10^{-2} cm^{-1} K^{-1})	χ_{Exp} (10^{-2} cm^{-1} K^{-1})	$\chi_{SCC-DFTB}$ (10^{-2} cm^{-1} K^{-1})	χ_{Exp} (10^{-2} cm^{-1} K^{-1})
$C_{10}H_8$		1.85 ± 0.23[b]		3.23 ± 0.75	
$C_{10}H_8^+$		2.60 ± 0.16		5.93 ± 0.15	
$[SiC_{10}H_8]^+$	$(C-H)_{Si}$	0.92 ± 0.28		6.94 ± 0.32	
	C−H	2.29 ± 0.30			
$C_{16}H_{10}$		1.85 ± 0.14	1.43(P)−1.69(H)	6.43 ± 0.29	
$C_{16}H_{10}^+$		2.35 ± 0.16		6.24 ± 0.17	
$[SiC_{16}H_{10}]^+$	$(C-H)_{Si}$	1.80 ± 0.26		6.49 ± 0.22	
	C−H	2.08 ± 0.25			
$C_{24}H_{12}$		1.94 ± 0.16	1.61(P)−2.30(H)	4.41 ± 0.21	3.82(P)−4.36(H)
$C_{24}H_{12}^+$		2.71 ± 0.15		5.36 ± 0.22	
$[SiC_{24}H_{12}]^+$	$(C-H)_{Si}$	1.39 ± 0.35		4.49 ± 0.77	
	C−H	2.07 ± 0.21			
$C_{32}H_{14}$		1.54 ± 0.12		5.84 ± 0.32	
$C_{32}H_{14}^+$		2.08 ± 0.13		5.79 ± 0.17	
$[SiC_{32}H_{14}]^+$	$(C-H)_{Si}$	1.23 ± 0.27		6.46 ± 0.26	
	C−H	1.77 ± 0.37			

[a] The available experimental values χ_{Exp} derived from measurements between 500 and 900 K by Joblin et al.[19] for neutral bare PAHs are also reported for comparison, the two values corresponding to peak (P) and midpoint at half maximum (H) measurements. [b] For comparison, value of Basire et al.:[13] 1.8×10^{-2} cm^{-1} K^{-1}

Complexes with Larger PAHs: IR Spectra Temperature Evolution. Dynamical spectra were calculated for complexes with larger PAHs (pyrene, coronene, and ovalene). For temperatures ranging from 10 to 900 K (10 to 600 K for $[SiC_{32}H_{14}]^+$), the system evaporated too fast at higher temperatures. All runs were performed starting from the lowest-energy isomer. The lowest temperature at which Si diffusion between minima is observed is ~400 K in the case of $[SiC_{10}H_8]^+$ for a simulation time of 100 ps. This threshold temperature is reduced for all the larger complexes (~300 K for $[SiC_{16}H_{10}]^+$; ~200 K for $[SiC_{24}H_{12}]^+$ and $[SiC_{32}H_{14}]^+$).

During the simulations, the Si atom remains on the edge of the PAH skeleton, on top of the external C−C bonds, the PES being flatter in this region (see for instance Figure 4 for the $[SiC_{24}H_{12}]^+$ complex). All the isomers probed during the dynamics are geometrically equivalent in the case of $[SiC_{10}H_8]^+$ and $[SiC_{24}H_{12}]^+$. Higher-energy isomers could be probed for $[SiC_{16}H_{10}]^+$ (two isomers of type **1** and four isomers of type **2**, cf. Figure 1) and $[SiC_{32}H_{14}]^+$ (four isomers of types **1**, **2**, and **3**).

At the highest temperature (900 K), the $[SiC_{16}H_{10}]^+$ complex geometry remains close to that of isomer **1** during 80% of the dynamics, isomer **1** being more stable by 0.22 eV than isomer **2**. Similarly, at 600 K, the $[SiC_{32}H_{14}]^+$ complex adopts a geometry close to that of the most stable isomer (**1**) during 90% of the simulation time. These time ratios are increased at lower temperatures, therefore all the other isomers have a low impact on the final spectra.

From a general point of view, the trends for the γ_{CH} and ν_{CC} band positions observed in the case of the $[SiC_{10}H_8]^+$ complex are similar for larger complexes. Redshifts of both γ_{CH} and ν_{CC} bands are observed. However, the broadenings due to the Si motion have lower amplitude for these larger systems.

Anharmonicity Factors. In this section, we report a quantitative study of the changes in the frequencies of the γ_{CH} and ν_{CC} modes as a function of temperature.

Benchmarking our theoretical approach was a challenge as very few experimental data are available. Experimental IR spectra for a set of neutral PAH (naphthalene, pyrene, coronene, and ovalene) have been recorded in the gas phase in a 500−900 K temperature range.[19] A linear variation of the band shifts as a function of temperature was shown. The empirical law for the band shifts

$$\nu(T) = \nu^{0K} - \chi T$$

was extracted, with χ being the anharmonicity factor that depends on the PAH and on the band.

To benchmark our model, we computed the anharmonic spectra of neutral PAHs between 10 and 900 K. To calculate the anharmonicity factors, the band positions were determined as follows: for each temperature, we computed five spectra and extracted the frequencies of the band maxima. The frequencies were then scaled (~1.1 for the γ_{CH} modes and 0.9 for the ν_{CC} modes) to fit the DFT harmonic band positions at 0 K. A linear evolution of the band shifts is obtained in the 10−900 K range, in agreement with the empirical law put forward by Joblin et al.[19] Average values were used for a weighted linear regression. The anharmonicity factors for the 10−900 K temperature range are reported in Table 3.

We find anharmonicity factors of (i) 1.85×10^{-2} cm^{-1} K^{-1} for the pyrene γ_{CH} mode, which compares well with the experimental value range ($1.43-1.69 \times 10^{-2}$ cm^{-1} K^{-1}); (ii) 1.94×10^{-2} cm^{-1} K^{-1} for the coronene γ_{CH} mode, which matches the experimental value range ($1.61-2.30 \times 10^{-2}$cm^{-1} K^{-1}); and (iii) 4.41×10^{-2} cm^{-1} K^{-1} for the coronene ν_{CC} mode, which is close to the experimental value range ($3.82-4.36 \times 10^{-2}$ cm^{-1} K^{-1}). For neutral naphthalene, no experimental data are available to our knowledge. However, the value we derived for the γ_{CH} mode (1.85×10^{-2} cm^{-1} K^{-1}) is very close to that calculated by Basire et al.[13] (1.8×10^{-2} cm^{-1} K^{-1}).

For all studied neutral PAHs, the anharmonicity factor of the ν_{CC} mode is larger than that of the γ_{CH} mode ($3.8-6 \times 10^{-2}$ cm^{-1} K^{-1} range vs $1.5-2.1 \times 10^{-2}$ cm^{-1} K^{-1}, cf. Table 3). Our results show that this trend is preserved in the case of PAH^+ and $[SiPAH]^+$ (cf. Table 3).

We now compare the neutral and cationic PAH spectral changes as a function of temperature. The anharmonicity factors for the γ_{CH} bands are systematically increased in the case of the cations by ~35% with respect to the neutrals. The effect

on the ν_{CC} bands depends on the PAH (almost no effect for $C_{16}H_{10}^+$ and $C_{32}H_{14}^+$ up to an increase of ~80% for $C_{10}H_8^+$). To our knowledge, no other theoretical or experimental data are available in the literature on charged PAHs for comparison.

Finally, we compare the cationic PAH^+ and $[SiPAH]^+$ spectral changes as a function of temperature. The γ_{CH} anharmonicity factor decreases upon Si-coordination by 23−65% for the $(C-H)_{Si}$ modes and by 12−24% for the (C−H) modes. The ν_{CC} anharmonicity is also affected by the coordination of Si, but not to such an extent. The ν_{CC} anharmonicity factor increases by 4−17% for all complexes except $[SiC_{24}H_{12}]^+$, for which a 16% decrease is found. However, the uncertainty on the $[SiC_{24}H_{12}]^+$ ν_{CC} anharmonicity factor, which is larger than those of the other complexes, does not enable us to disentangle a trend for this particular species.

Astrophysical Implications. Our previous paper pointed out characteristic features of Si coordination to PAH based on DFT harmonic frequency calculations. It led to a possible assignment of the blue wing of the 6.2 μm AIB (1610 cm^{-1}) and of the AIB satellites at 6.0 μm (1670 cm^{-1}) and 11.0 μm (900 cm^{-1}) to $[SiPAH]^+$ complexes. The calculation of anharmonic spectra in the present study brings new spectroscopic constraints to this assignment.

To estimate the emission temperatures of $[SiPAH]^+$ in the ISM, one has to consider the spectral distribution of the radiation field and exclude photons that lead to photodissociations. In a previous experimental study of the $[FeC_{24}H_{12}]^+$ complex, it was shown that the dissociation threshold is reached at 5 eV[58] or a temperature of 1100 K in a harmonic microcanonical description. Considering that the Fe-$C_{24}H_{12}^+$ binding energy is estimated at about 2.6 eV, a Si-$C_{24}H_{12}^+$ binding energy of 2.0 eV should necessarily induce the loss of Si at somewhat lower temperature. This is consistent with the difficulties that we met to perform simulations of 100 ps durations at 900 K for the $[SiC_{24}H_{12}]^+$ and at temperatures ranging from 600 to 900 K for the $[SiC_{32}H_{14}]^+$ due to Si evaporation, as mentioned previously.

In a given radiation field, we therefore expect the range of temperatures involved in the emission process to be more limited for a $[SiPAH]^+$ cation than for its PAH counterpart. If we further consider the significantly reduced anharmonicity factors for the $(C-H)_{Si}$ bends as compared with that of the γ_{CH} mode of PAH^+, we can predict that the satellite band at 11.0 μm that has been assigned to $[SiPAH]^+$ complexes should be less affected by local physical conditions than the 11.2 μm AIB.

Conclusions

The anharmonic effects on the γ_{CH} and ν_{CC} bands in the mid-IR spectra of $[SiPAH]^+$ complexes have been determined by molecular dynamics simulations on a SCC-DFTB PES with modified parameters. These studies show that:

(i) the coordination of Si induces an enhanced broadening of both bands, and a modification of the shape of the γ_{CH} bands due to couplings to soft modes associated with the motion of Si.

(ii) systematic redshifts occur, following a linear law for PAH, PAH^+, and $[SiPAH]^+$ that enables anharmonicity factors to be extracted.

(iii) the coordination of Si leads to a decrease of the anharmonicity factor for the γ_{CH} mode, all the more as the H atom is close to the Si atom, and to a slight increase of the anharmonicity factor for the ν_{CC} mode.

The approach used in this work has been benchmarked on bare neutral PAH as no experimental IR spectra of $[SiPAH]^+$ complexes have been reported in the literature to our knowledge.

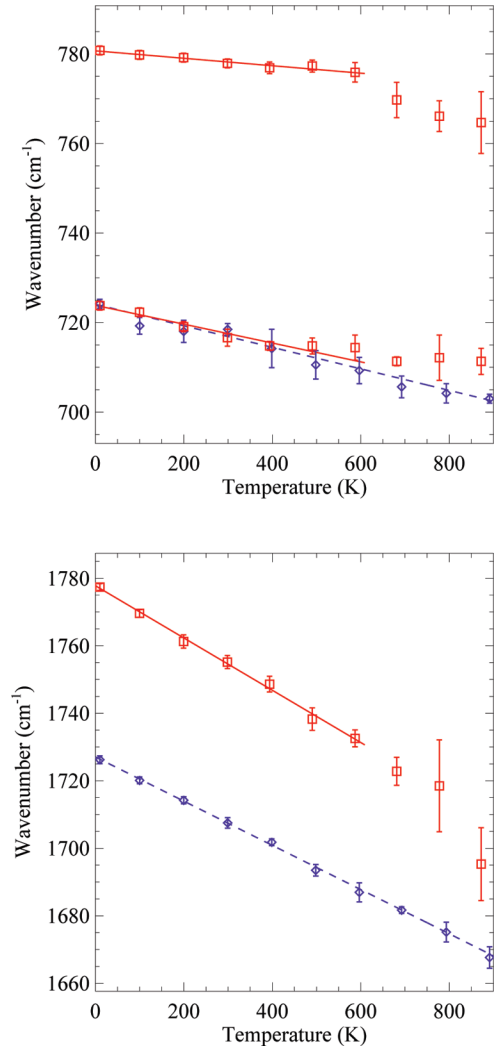

Figure 10. Variations of the γ_{CH} band positions (up) and ν_{CC} band positions (down) as a function of the temperature for $C_{10}H_8^+$ (dashed) and $[SiC_{10}H_8]^+$ (continuous). Diamonds and squares: mean positions at maximum intensity of the bands for $C_{10}H_8^+$ and $[SiC_{10}H_8]^+$, respectively.

Such experimental data would be of primary interest to confirm the results presented here. In the present study, all the spectra were obtained from molecular dynamics performed in the microcanonical ensemble. It would be interesting to compare them with spectra derived from molecular dynamics in the canonical ensemble. We also note that the anharmonic zero-point effect should be taken into account. This was done previously by Van-Oanh et al.[16] for neutral naphtalene using the adiabatic switching approach. Path-integral methods[59−61] may offer another alternative. Clearly, other types of simulations with more elaborate calculations of the electronic structure or addressing quantum dynamics would be of interest to confirm the present results.

These results bring new molecular data for the infrared spectroscopic characterization of hot $[SiPAH]^+$ complexes that are of interest for laboratory experiments such as infrared multiple photodissociation spectroscopy and for their identification in the interstellar medium. A further step to test the assumption of their presence in such a medium will be to characterize the equilibrium between the formation and destruction of these species under interstellar conditions. This involves the investigation of reactivity and fragmentation processes at the molecular level.

Acknowledgment. The authors thank the French national program "Physique et Chimie du Milieu Interstellaire" and the cluster research group GDR 2758 for their support, as well as the CALMIP platform for providing computational facilities. P. Parneix and T. Heine are also acknowledged for fruitful discussions. Special thanks to J. Aumont for the nice weighted fits.

References and Notes

(1) Joblin, C.; Léger, A.; Martin, P. *Astrophys. J. Lett.* **1992**, *393*, L79–L82.
(2) Léger, A.; Puget, J. L. *Astron. Astrophys.* **1984**, *137*, L5–L8.
(3) Allamandola, L. J.; Tielens, A. G. G. M.; Barker, J. R. *Astrophys. J. Lett.* **1985**, *290*, L25–L28.
(4) Whittet, D. C. B. *Dust in the galactic environment*, 2nd ed; Whittet, D. C. B. Ed.; Institute of Physics (IOP) Publishing: Bristol, 2003; 2003 Series in Astronomy and Astrophysics.
(5) Joalland, B.; Simon, A.; Marsden, C. J.; Joblin, C. *Astron. Astrophys.* **2009**, *494*, 969–976.
(6) Bohme, D. K.; Wlodek, S.; Wincel, H. *J. Am. Chem. Soc.* **1991**, *113*, 2802–2806.
(7) Srinivas, R.; Hrusak, J.; Sulzle, D.; Bohme, D. K.; Schwarz, H. *J. Am. Chem. Soc.* **1992**, *114*, 2802–2806.
(8) Jaeger, J. B.; Pillai, E. D.; Jaeger, T. D.; Duncan, M. A. *J. Phys. Chem. A* **2005**, *109*, 2801–2808.
(9) Dunbar, R. C.; Uechi, G. T.; Asamoto, B. *J. Am. Chem. Soc.* **1994**, *116*, 2466–2470.
(10) Pozniac, B. P.; Dunbar, R. C. *J. Am. Chem. Soc.* **1997**, *119*, 10439–10445.
(11) Bohme, D. K.; Wlodek, S.; Wincel, H. *Astrophys. J. Lett.* **1989**, *342*, L91–L93.
(12) Léger, A.; D'Hendecourt, L.; Boissel, P.; Désert, F. X. *Astron. Astrophys.* **1989**, *213*, 351–359.
(13) Basire, M.; Parneix, P.; Calvo, F.; Pino, T.; Bréchignac, P. *J. Phys. Chem. A* **2009**, *113*, 6947–6954.
(14) Pirali, O.; Vervloet, M.; Mulas, G.; Malloci, G.; Joblin, C. *Phys. Chem. Chem. Phys.* **2009**, *11*, 3443–3454.
(15) Basire, M.; Parneix, P.; Calvo, F. *J. Chem. Phys.* **2008**, *129*, 081101.
(16) Van-Oanh, N. T.; Parneix, P.; Brechignac, P. *Phys. Chem. Chem. Phys.* **2005**, *7*, 1779–1784.
(17) Cook, D. J.; Schlemmer, S.; Balucani, N.; Wagner, D. R.; Harrison, J. A.; Steiner, B.; Saykally, R. J. *J. Phys. Chem. A* **1998**, *102*, 1465–1481.
(18) Van Oanh, N. T.; Parneix, P.; Bréchignac, P. *J. Phys. Chem. A.* **2002**, *106*, 10144–10151.
(19) Joblin, C.; Boissel, P.; Léger, A.; D'Hendecourt, L.; Defourneau, D. *Astron. Astrophys.* **1995**, *299*, 835–846.
(20) Williams, R. M.; Leone, S. R. *Astrophys. J.* **1995**, *443*, 675–681.
(21) Schlemmer, S.; Cook, D.; Harrison, J.; Wurfel, B.; Chapman, W.; Saykally, R. *Science* **1994**, *265*, 1686–1689.
(22) Herman, M.; Lievin, J.; Auwera, J. V.; Campargue, A. *Global and Accurate Vibration Hamiltonians from High Resolution Molecular Spectroscopy*; Wiley: New York, 1999.
(23) Manthe, U.; Meyer, H.-D.; Cederbaum, L. S. *J. Chem. Phys.* **1992**, *97*, 3199–3213.
(24) Beck, M. H.; Jackle, A.; Worth, G. A.; Meyer, H. D. *Phys. Rep.* **2000**, *324*, 1–105.
(25) Vendrell, O.; Gatti, F.; Meyer, H.-D. *J. Chem. Phys.* **2007**, *127*, 184303.
(26) Cané, E.; Miani, A.; Trombetti, A. *J. Phys. Chem. A* **2007**, *111*, 8218–8222.
(27) Merrick, J. P.; Moran, D.; Radom, L. *J. Phys. Chem. A* **2007**, *111*, 11683–11700.
(28) Estacio, S. G.; Cabral, B. J. C. *Chem. Phys. Lett.* **2008**, *456*, 170–175.
(29) Kumar, P.; Marx, D. *Phys. Chem. Chem. Phys.* **2006**, *8*, 573–586.
(30) Gaigeot, M.-P.; Sprik, M. *J. Phys. Chem. B* **2003**, *107*, 10344–10358.
(31) Porezag, D.; Frauenheim, T.; Köhler, T.; Seifert, G.; Kaschner, R. *Phys. Rev. B* **1995**, *51*, 12947.
(32) Seifert, G.; Porezag, D.; Frauenheim, T. *Int. J. Quantum Chem.* **1996**, *58*, 185–192.
(33) Elstner, M.; Porezag, D.; Jungnickel, G.; Elsner, J.; Haugk, M.; Frauenheim, T.; Suhai, S.; Seifert, G. *Phys. Rev. B* **1998**, *58*, 7260–7268.
(34) Oliveira, A.; Seifert, G.; Heine, T.; duarte, H. *J. Braz. Chem. Soc.* **2009**, *20*, 1193.
(35) Rauls, E.; Elsner, J.; Gutierrez, R.; Frauenheim, T. *Sol. State Comm.* **1999**, *111*, 459–464.
(36) Sieck, A.; Frauenheim, T.; Jackson, K. A. *Phys. Stat. Sol. (b)* **2003**, *240*, 537–548.
(37) Anisimov, V. I.; Aryasetiawan, F.; Lichtenstein, A. I. *J. Phys. Cond. Matt.* **1997**, *9*, 767–808.
(38) Mosey, N. J.; Carter, E. A. *Phys. Rev. B* **2007**, *76*, 155123.
(39) Kotliar, G.; Savrasov, S. Y.; Haule, K.; Oudovenko, V. S.; Parcollet, O.; Marianetti, C. A. *Rev. Mod. Phys.* **2006**, *78*, 865–951.
(40) McQuarrie, D. A. *Statistical Mechanics*; Harper and Row ed.: New York, 1976.
(41) Pech, C.; Joblin, C.; Boissel, P. *Astron. Astrophys.* **2002**, *388*, 639–651.
(42) Kalinowski, J.; Lesyng, B.; Thompson, J.; Cramer, C.; Truhlar, *J. Phys. Chem. A* **2004**, *108*, 2545–2549.
(43) Li, J.; T., Z.; Cramer, C. J.; Truhlar, D. G. *J. Phys. Chem. A* **1998**, *102*, 1820–1831.
(44) Winget, P.; D., T. J.; Xidos, J. D.; Cramer, C. J.; Truhlar, D. G. *J. Phys. Chem. A* **2002**, *106*, 10707–10717.
(45) Thompson, J. D.; Cramer, C. J.; Truhlar, D. G. *J. Comput. Chem.* **2003**, *24*, 1291–1304.
(46) Rapacioli, M.; Spiegelman, F.; Talbi, D.; Mineva, T.; Goursot, A.; Heine, T.; Seifert, G. *J. Chem. Phys.* **2009**, *130*, 244304.
(47) Vigne-Maeder, F.; Claverie, P. *J. Chem. Phys.* **1988**, *88*, 4934–4948.
(48) Gordon, M. S.; Freitag, M. A.; Bandyopadhyay, P.; Jensen, J. H.; Kairys, V.; Stevens, W. J. *J. Phys. Chem. A* **2000**, *105*, 293–307.
(49) Derepas, A.-L.; Soudan, J.-M.; Brenner, V.; Dognon, J.-P.; Millié, P. *J. Comput. Chem.* **2002**, *23*, 1013–1030.
(50) Liem, S. Y.; Popelier, P. L. A. *J. Chem. Phys.* **2003**, *119*, 4560–4566.
(51) Ren, P.; Ponder, J. W. *J. Phys. Chem. B* **2003**, *107*, 5933–5947.
(52) Piquemal, J.-P.; Gresh, N.; Giessner-Prettre, C. *J. Phys. Chem. A* **2003**, *107*, 10353–10359.
(53) Gresh, N.; Cisneros, G. A.; Darden, T. A.; Piquemal, J.-P. *J. Chem. Theo. Comp.* **2007**, *3*, 1960–1986.
(54) Hudgins, D. M.; Sandford, S. A. *J. Phys. Chem. A* **1998**, *102*, 329–343.
(55) Cimas, A.; Vaden, T. D.; de Boer, T. S. J. A.; Snoek, L. C.; Gaigeot, M. P. *J. Chem. Theo. Comp.* **2009**, *5*, 1068–1078.
(56) Gregoire, G.; Gaigeot, M. P.; Marinica, D. C.; Lemaire, J.; Schermann, J. P.; Desfrancois, C. *Phys. Chem. Chem. Phys.* **2007**, *9*, 3082–3097.
(57) Marinica, D. C.; Grégoire, G.; Desfrancois, C.; Schermann, J. P.; Borgis, D.; Gaigeot, M. P. *J. Phys. Chem. A* **2006**, *110*, 8802–8810.
(58) Simon, A.; Joblin, C. *J. Phys. Chem. A* **2009**, *113*, 4878–4888.
(59) Ramírez, R.; López-Ciudad, T.; P, P. K.; Marx, D. *J. Chem. Phys.* **2004**, *121*, 3973–3983.
(60) Shiga, M.; Nakayama, A. *Chem. Phys. Lett.* **2008**, *451*, 175–181.
(61) Kaczmarek, A.; Shiga, M.; Marx, D. *J. Phys. Chem. A* **2009**, *113*, 1985–1994.

JP911526N